ELSEVIER

Polymer 42 (2001) 4537–4548

polymer

www.elsevier.nl/locate/polymer

Structure development and properties of PET fibre filled PP composites

C. Saujanya, S. Radhakrishnan*

Polymer Science and Engineering, National Chemical Laboratory, Council of Scientific and Industrial Research, Pune 411008, India

Received 3 July 2000; received in revised form 23 October 2000; accepted 1 November 2000

Abstract

The structure development and mechanical properties of polypropylene (PP) composite containing polyethylene terephthalate (PET) fibres were studied both in the presence and absence of a compatibilizer such as maleic anhydride (MA). The structural and morphological studies were carried out by WAXD, optical microscopy and SEM techniques. In the absence of MA, the PET fibres in PP showed transcrystalline morphology and thus proved to be a strong nucleating agent for PP spherulites. On the other hand, in the presence of MA, no transcrystalline growth of PP was observed on the surface of PET fibres. The fibre to matrix bonding was better in presence of MA than without it, as was revealed by SEM of fractured surfaces. The mechanical properties viz. impact strength and tensile modulus showed enhancement for these composites as compared to pure PP. However, pronounced increase in the properties was seen for PET fibres filled PP composite without MA. The above findings could be understood in terms of high aspect ratio for PET fibres, transcrystalline morphology, good fibre–matrix adhesion and nucleating ability of PET fibres in PP matrix.

Keywords: Transcrystalline morphology; Polyethylene terephthalate; Nucleating ability

1. Introduction

Fibres have been used for improving the strength and rigidity of polymers. Numerous studies have been reported concerning the reinforcement of polypropylene (PP) and other thermoplastic polymers using different types of fibres in order to achieve improvement in tensile modulus [1–3]. Amongst the various fibres that have been used, the studies on PP filled with glass fibres are the most common [4,5]. Some of the fibres induce transcrystalline morphology as has been recently reported to occur in PP when melt crystallised in contact with carbon, aramid [6,7] as well as other polymeric fibres [8–12]. Such transcrystalline morphology has also been observed in many other semi-crystalline polymers including polyphenelene sulphide (PPS) [13], polyether ketone (PEK) [13], Nylon 6 [14], Nylon 66 [3], polyethylene terephthalate (PET) [15,16] and polyether ether ketone (PEEK) [17]. Apart from the morphological studies, the importance of transcrystalline interface on the mechanical properties of some fibre reinforced polymer systems was also investigated. In case of carbon fibre reinforced PEEK [17–19], the formation of transcrystalline morphology showed higher interfacial bond strength and high transverse tensile strength. As regards glass fibres, it is not very clear whether it induces transcrystallinity in PP. Some authors contend that it affects crystallisation behaviour of PP while others propose that the shearing action/movement of glass fibres causes changes in the morphological features in glass filled PP [20]. It is also not clear as yet whether the development of transcrystalline phase are important for the mechanical properties of fibre-filled PP composites. The main reason for this has been that the glass fibres are amorphous, supplied by different manufacturers with various types of sizing, finishing, etc.

Hence, it was proposed to study PET fibre filled PP composites since the PET fibre offers various advantages over other fibres: (a) It is available in well defined form without sizing. (b) It has a well-defined structure with low density and a high modulus of 2758 MPa. (c) The most important of all is that it exhibits transcrystalline morphology in PP. (d) The PP/PET interface can be modified by using compatibilizer. In the present article, results on our investigation on the structure development of PP at PET interface, i.e. the crystallisation behaviour, trancrystalline morphology and kinetics of crystallisation as well as its effect on mechanical properties are described. The effect of compatibilizer, i.e. maleic anhydride (MA) on the structure and properties of PET fibre filled PP composite system (PP/PET) are also included.

2. Experimental

In order to study the crystallisation behaviour of PP in presence of PET fibres, the commercial PP (Koylene grade

* Corresponding author. Tel.: +91-212-331-453; fax: +91-212-334-761.
E-mail address: prs@ems.ncl.res.in (S. Radhakrishnan).

0032-3861/01/$ - see front matter
PII: S0032-3861(00)00860-0

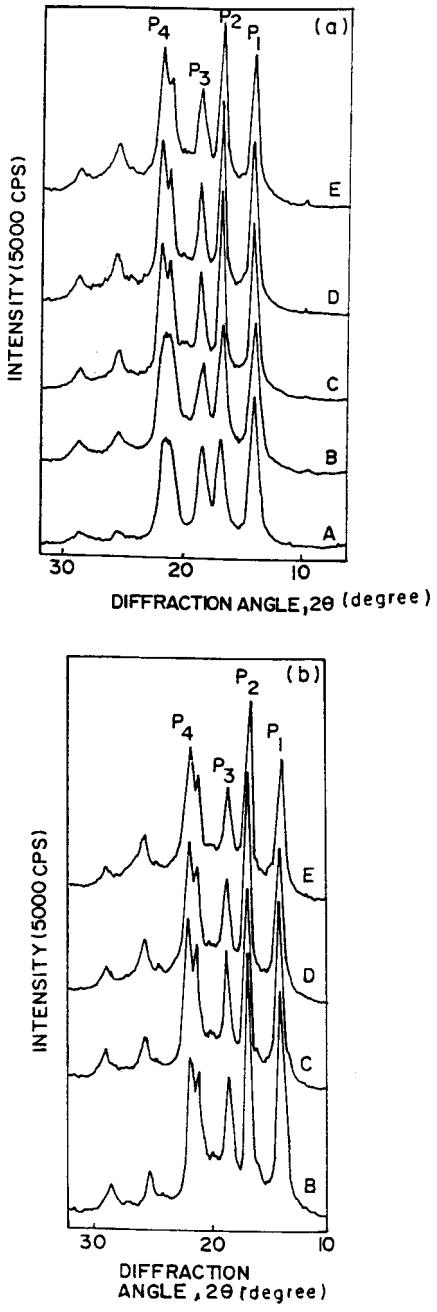

Fig. 1. WAXD scans for PET fibre filled PP composite isothermally melt crystallised at: (a) $T_c = 110°C$; and (b) 115°C. Curves B–E correspond to PET fibre concentration of 2, 4, 7 and 11 wt%, respectively, while curve A corresponds to that of pure PP.

SM030, IPCL, Baroda, MFI-8-10) was first precipitated in powder form by dropping its xylene solution into acetone and subsequently filtering and drying the same in vacuum (10^{-2} Torr) for 24 h. This pure powder was then mixed with the PET fibres (Terene Fibres Ltd, POY, strength 120 g/denier, 15 μm diameter) chopped to 4–5 mm length in the desired proportions ranging from 2 to 16.6 wt%. A small quantity of each composition was melted on a glass slide at 200°C and kept for 1–2 min to allow wetting of the fibres (since the melting point of PET is much higher than 200°C, the fibres remain intact). The isothermal crystallisation behaviour was studied at crystallisation temperatures of 100, 105, 110 and 115°C, respectively. The spherulitic growth rate was monitored with respect to time at a constant crystallisation temperature by continuously recording the images using a video camera attached to a polarising optical microscope (Leitz, Germany). These were subsequently analysed in the selected area close to PP/fibre interface for changes in the intensity or grey scale using image analyser system (VIDPRO 32, Leading Edge, Australia). These were also compression moulded in a single ended compaction die at 29 MPa pressure for 30 s to form thin discs (12 mm diameter, 2 mm thick) which were subjected to melt crystallisation on the hot stage (melt temperature 190°C; crystallisation at 115°C; time, 20 min) of optical microscope and further quenched in methanol. The structure and morphology were investigated by XRD and optical microscopy in the same manner as reported elsewhere [21–23].

In another set, PP was mixed with a compatibilizer, i.e. maleic anhydride (MA) in different concentrations of 5, 10 and 15 wt%. The samples were heated to the melting point of PP so as to obtain MA grafted PP (PP-*g*-MA). The PET fibres were added in desired quantity to the sample during the process. The crystallisation behaviour of these samples was studied in the same manner as described above. Some of the PP/PET composites (compatibilised with and without MA) were extruded at a mild extrusion rate of 2 g/min from a melt indexer at a temperature of 190°C. A thin section of these samples were observed under SEM in order to determine the morphological changes during melt processing. The DSC studies were carried out for these composites for determining the trancrystalline phase using T_c and T_m.

Mechanical properties such as impact and tensile modulus were investigated for these composites. The commercially available PP pellets were mixed with PET fibres chopped to 3 cm length in the desired proportions and first compounded using Brabender Plasticorder Single screw Extruder (SSE). Another set was made where the MA was first added to PP at 10 wt% concentration and then PET fibres were mixed and compounded as described before. The temperature conditions set in the SSE were same as reported earlier [24]. The screw speed was maintained at 14–16 rpm for PP/PET and 20 rpm for PP-*g*-MA/PET. The samples thus extruded were pelletised, dried and injection moulded in the same manner as described earlier. The notched impact (ASTM-256) [25] and tensile properties (ASTM-638) [26] of the moulded specimens were measured. Approximately 8–10 samples were tested for each composition and the average values obtained for different parameters are reported here in this paper. The tests were performed at ambient temperatures (30°C) and humidity conditions. The complete details of specifications of techniques used for investigation of properties were same as described in the previous reports [27,28]. The resultant properties obtained were correlated with the structure and morphology of the composite.

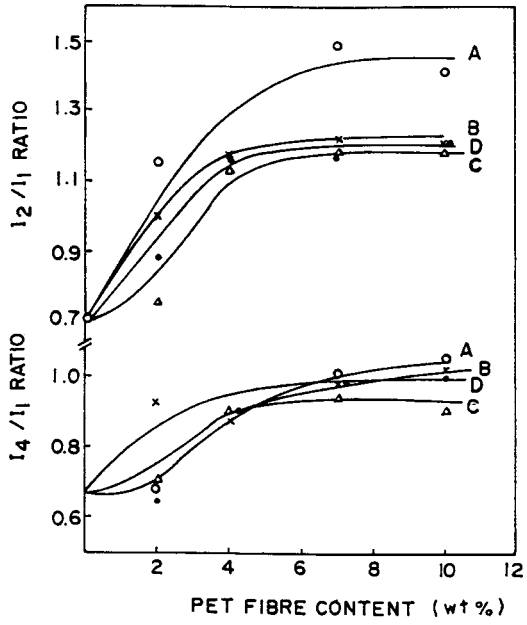

Fig. 2. The variation of intensities of P_2 and P_4 peaks in relation to P_1 peak as a function of PET fibre content. Curves A–D correspond to samples crystallised at T_c of 115, 110, 105 and 100°C, respectively.

3. Results and discussion

3.1. Structure and morphology in PET fibre filled PP

Fig. 1 shows the wide angle X-ray diffraction (WAXD) for PP containing different concentrations of PET fibres.

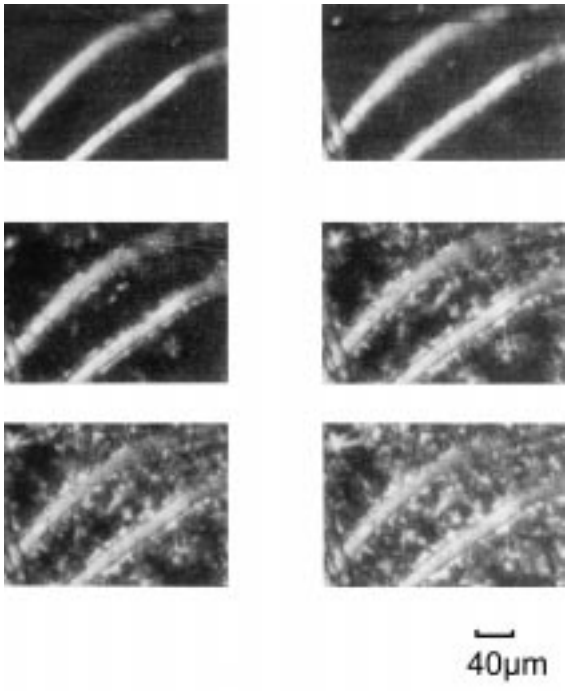

Fig. 3. Optical micrograph of PP containing 10 wt% PET fibre at various stages of crystallisation at $T_c = 115°C$. (net magnification = 1000×)

The crystallisation behaviour was studied at crystallisation temperatures (T_c) of 100, 105, 110 and 115°C but here we have shown the results only at 110 and 115°C. In these figures, curves B–E correspond to PET fibre concentration in the range of 2, 4, 7 and 11 wt%, respectively, while curve A corresponds to that of pure PP. The XRD scans reveal identical reflections corresponding to monoclinic α-crystalline phase of PP at all concentrations of PET. However, the intensities of peaks change considerably depending on the concentration of PET fibres. In case of pure disoriented PP having α phase, the intensity of (110) reflection at 2θ of 14.2° (peak 1) is usually the highest. On the other hand, with an increase in the concentration of PET fibres, the intensity of (040) reflection occurring at 2θ of 16.7° (peak 2) becomes higher than the rest. The peak at 2θ of 21.7° corresponding to (041) reflection (peak 4) is also affected by the presence of PET fibres.

The variations of intensities of these peaks (P_2, P_4) in relation to peak P_1 as a function of concentration of PET fibres are shown in Fig. 2. Curves A–D correspond to samples crystallised at T_c of 100, 105, 110 and 115°C, respectively. It is clear from this figure that the intensity of (040) reflection (P_2) increases appreciably with the increase of PET fibre concentration and shows a maximum intensity at about 7 wt% of PET. The intensity of (041) reflection (P_4) also shows similar behaviour. Since the intensity of (040) and (041) reflections are mainly affected by the presence of PET, it can be concluded that the growth of PP crystallites along the *b*-axis is considerably affected by the presence of PET fibres.

Fig. 3 shows the optical polarising micrographs of the PP samples containing 10wt.% PET fibres at various stages of $T_c = 115°C$. It is evident from these micrographs that extensive nucleation is observed first at the fibre surface giving rise to columnar growth or transcrystalline phase of PP at the PET fibre surface. The normal PP spherulites are seen to appear at a region away from the interface much later than the nucleation period of the transcrystalline phase.

The kinetics of crystallisation in the transcrystalline zone was monitored by the spot intensity measurements under cross-polar conditions (at the selected area on the images recorded by the video camera attached to the microscope). Fig. 4 shows the crystallisation of PP by a plot of intensity as a function of time at $T_c = 115°C$. The curves A–D correspond to the crystallisation of PP near the fibre interface with a PET concentration of 2, 4, 7 and 11 wt%, respectively, while the curve E corresponds to the crystallisation of PP away from the fibre (in the normal bulk). By comparing the curves, it is evident that the crystallisation process at the fibre interface or transcrystalline zone is much faster than that in the bulk. The crystallisation half time ($t_{1/2}$) and crystallisation rate were determined from these curves for the various crystallisation temperatures (T_c) of 105, 110 and 115°C, which are shown in Fig. 5a and b. There is a remarkable decrease in the $t_{1/2}$ values as compared to pure PP which is clearly observed at $T_c = 115°C$. The $t_{1/2}$ initially decreases

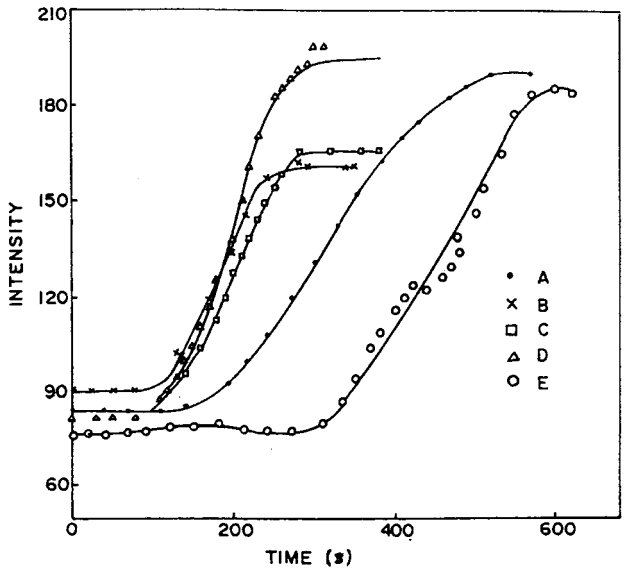

Fig. 4. Transmitted intensity (under X polars) as a function of time for PP/PET isothermally crystallised at 115°C. Curves A–D correspond to PET fibre concentration of 2, 4, 7 and 11 wt%, respectively, and curve E corresponds to that of pure PP.

and then attains a limiting value of 160, 100 and 40 s for T_c of 115, 110 and 105°C, respectively, with an increase in the fibre concentration up to 16.6 wt%. The growth rate is also high for the crystals growing near the PP/PET fibre interface as compared to PP crystals growing at places away from the interface (see Fig. 5b). The growth rate increases by increasing the PET fibre concentration by 7–10 wt% and then attains a limiting value above this concentration. These findings clearly suggest that the PET fibre initiates heterogeneous nucleation in the PP matrix giving rise to first transcrystalline morphology at the fibre interface followed by subsequent growth of crystallisation in bulk.

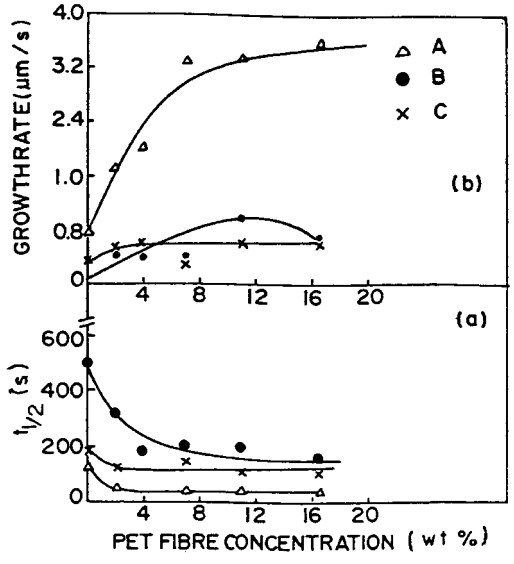

Fig. 5. The crystallisation half time, $t_{1/2}$: (a) and growth rate; (b) of PP as a function of PET fibre content. Curves A, B and C correspond to T_c at 105, 110 and 115°C.

Fig. 6 shows the variation of crystallinity as a function of PET fibre content determined from the XRD scans. It can be seen that the crystallinity is much higher in presence of PET fibres, which increases from 62% in virgin disoriented PP to 75% in PP/PET. This enhancement of the crystallinity value clearly suggests preferential nucleation of PP on the surface of PET fibres giving rise to transcrystalline morphology. Thus, from the crystallisation half time, growth rate and crystallinity, and intensities of certain reflections in XRD it can be concluded that there is considerable interaction between the PET fibre and PP matrix.

The crystallisation kinetics for both for normal PP spherulites as well as in the transcrystalline phase were analysed according to the Avrami equation [29].

$$\log[(I_m - I_t/I_m - I_o)] = A_v t^n K \quad (1)$$

or

$$\log \log[I_m - I_t/I_m - I_o] = A_v n \log t + C$$

where I is the intensity value through the cross polar due to the formation of crystallites. A_v and K are constants and n is the Avrami exponent. The subscripts t, m and o denote the corresponding values of I at time t, $t = m$ and $t = o$, respectively. Fig. 7 shows the Avrami plot of log (fractional conversion) vs time on the log–log scale. Curves A and B represent the Avrami plots of PP/PET and pure PP at 115°C, respectively. The values of n were found to be about 3 for normal PP and 4–4.5 for the transcrystalline phase of PP grown at PET interface. The higher value of n for the transcrystalline phase clearly indicates the heterogeneous nucleation and linear growth of the crystallites. Turnbull and Vonnegut [30] have attributed the presence of transcrystalline phase to the closeness of match between the lattice parameters of substrate and polymer matrix crystals. Thus the development of transcrystallinity may be associated with the oriented overgrowth of PP crystallites on PET

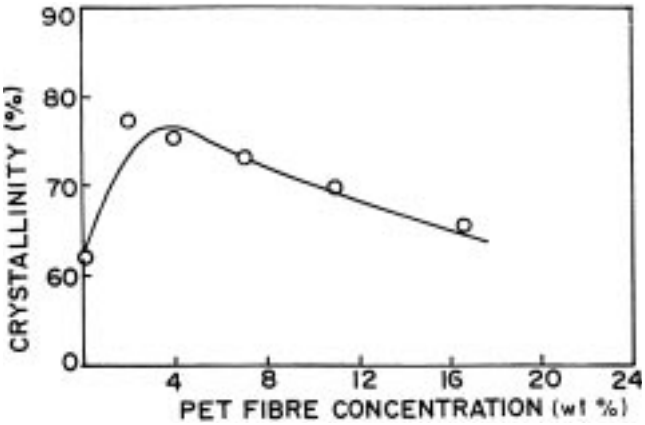

Fig. 6. The variation of crystallinity (%) as a function of PET fibre content at $T_c = 115°C$.

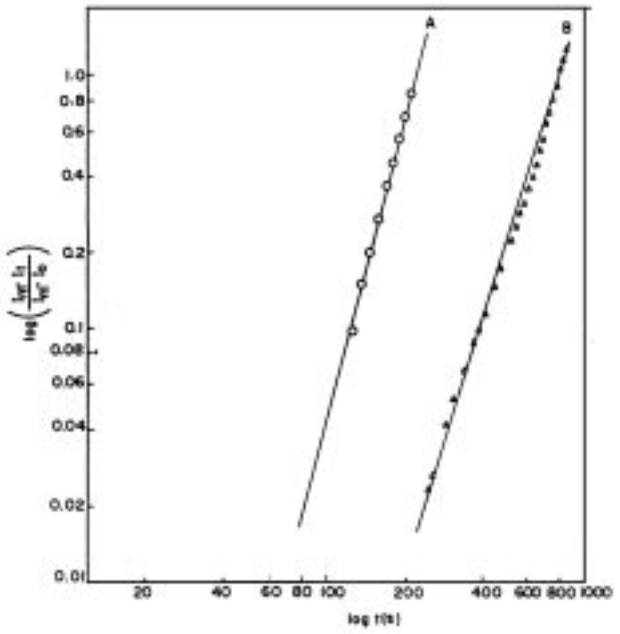

Fig. 7. Avrami plot of log (fractional conversion)vs time on log–log scale. Curve A = PP/PET at $T_c = 115°C$ and curve B = pure PP.

fibres. According to lattice mismatch theory, if the mismatch parameter (δ) defined as

$$\delta_1 = |pl_s - ql_g|/|l_s| \times 100 \quad (2)$$

where L is the lattice parameter along any axis; p and q are integers. The subscripts s and g represent substrate and growing media, which if is less than 10% then there is a preferential growth or even epitaxial growth of one phase over the other.

If one considers the lattice parameters of the α phase of PP $a = 6.5$ Å, $b = 20.9$ Å $c = 6.5$ Å and $\beta = 99.3°$ with those of PET ($a = 4.56$ Å, $b = 5.94$ Å, $c = 10.75$ Å and $\alpha = 98.5°$, $\beta = 118°$, $\gamma = 112°$. The lattice mismatch between b-axis of PP and $2 \times c$-axis of PET is less than 3% while that between c-axis of PP and b-axis of PET is less than 8.5%. Hence it is quite likely that the $\{bc\}$ planes of the PP crystals get aligned initially along the fibre axis of PET fibres and subsequently these crystals grow with preferential b-axis orientation. The alignment of b-axis of crystallites gives rise to change in the intensity of (040) reflection as observed in this case. These observations clearly indicate that since there is preferential orientation of b-axis and/or bc planes of PP crystallites along the c-axis of PET fibre, the crystal structure of fibre material could also be important for the development of transcrystalline phase.

3.2. Structure and morphology in PP-g-MA/PET

The studies of PP composite containing PET fibres compatibilised with maleic anhydride were investigated. Fig. 8 shows the WAXD scans for the PP-g-MA/PET with

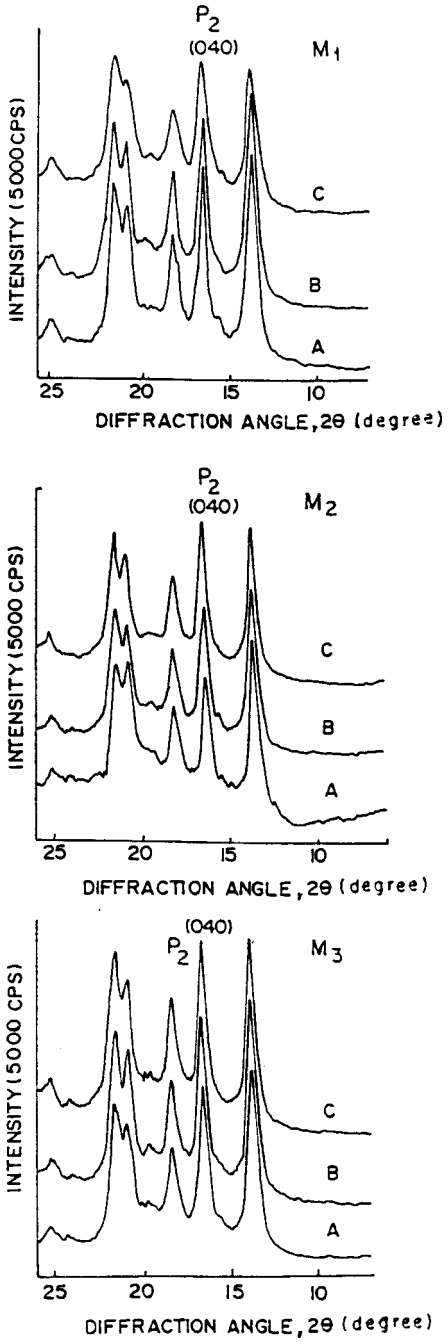

Fig. 8. WAXD scans for PP-g-MA/PET. Symbols M_1, M_2 and M_3 correspond to MA concentration of 5, 10 and 15 wt%. Curves A, B and C correspond to PET fibre concentration of 4, 7 and 11 wt%, respectively.

10 wt% concentration of MA isothermally crystallised from melt at T_c of 115°C as a function of PET concentration. Symbols M_1, M_2 and M_3 correspond to MA concentration of 5, 10 and 15 wt% and curves A–C correspond to PET concentration of 4, 7 and 11 wt%, respectively. In all the cases, characteristic diffraction maxima of monoclinic α form of PP are obtained. However, the intensity of peak at 2θ of 16.7° due to (040) reflection remains almost

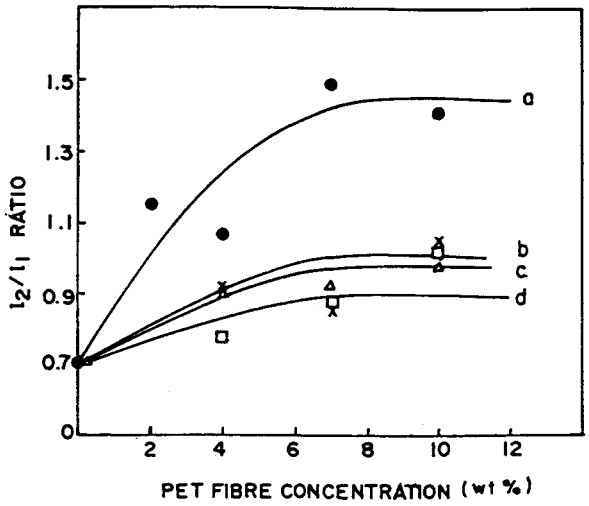

Fig. 9. Change of intensity of P_2 peak in relation to P_1 peak as a function of PET fibre content in PP-*g*-MA/PET composites. Curve A corresponds to without MA and curves B–D contain MA concentration of 5, 10 and 15 wt%, respectively.

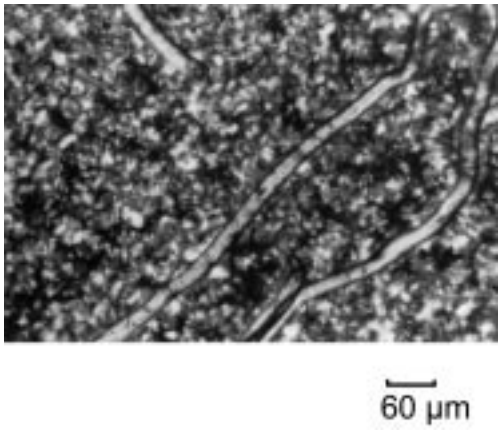

Fig. 10. Optical micrograph of PP-*g*-MA with 7% PET containing 10% MA isothermally crystallised at $T_c = 115°C$. (net magnification = 450 ×).

unaffected in presence of MA with varying PET fibre content.

Fig. 9 shows the variation of intensity of peak (P_2) in relation to P_1 peak ($2\theta = 14°$, 110 reflection) as a function of PET fibre content at 115°C. Curve A shows the PP/PET without MA while curves B–D correspond to PP/PET with 5, 10 and 15 wt% concentration of MA. The peak intensity (P_2) corresponding to 040 reflection is suppressed for the curves B–D containing MA while in the absence of MA (curve a), the peak intensity of (040) reflection is appreciably high and it increases with increase of PET fibre content as explained earlier. The decrease in the intensity of P_2 peak for PP/PET with MA compared to PP/PET without MA shows that there is no preferential orientation of *b*-axis in presence of maleic anhydride. The suppression of *b*-axis (040 peak intensity) can be associated with the absence of transcrystalline phase. We confirmed this result in a later section using the crystallisation behaviour and morphological studies of this system.

The optical micrograph of PP with 7 wt% PET containing 10 wt% MA isothermally crystallised at $T_c = 115°C$ is shown in Fig. 10. Extensive nucleation is observed both at the fibre surface and as well as in the bulk at the same time (away from fibre interface). The spherulites are considerably smaller than 15 μm. It is also interesting to note that no transcrystalline morphology is observed at the fibre surface.

Fig. 11 shows the WAXD scans for PP with 7 wt% PET fibre with varying concentration of MA from 5 to 15 wt% at $T_c = 115°C$. With the increase in concentrations of MA, the intensity of P_2 peak at 2θ of 16.7° due to the (040) reflection of the α phase of PP remain practically constant with respect to P_1 peak ($2\theta = 14°$, 110 reflection). This shows that the intensity of (040) reflection of peak 2 is unaffected with an increase in the MA concentration.

The isothermal crystallisation behaviour was monitored by a plot of intensity as a function of time for PP/PET fibre containing 10 wt% concentration of MA, which is shown in Fig.12. The curves A, B and C correspond to PET fibre concentration of 4, 7 and 11 wt% with respect to PP. It is evident that the crystallisation processes in the bulk as well as along the fibre surface are similar with no transcrystalline zone. The induction period is much smaller than that of pure PP. The crystallisation half time and the crystallisation growth rates were determined from these curves, which are shown in Fig. 13a and b. The curves A and B show the $t_{1/2}$ and growth rate values for PP/PET without MA and PP/PET containing 10 wt% MA, respectively. Considerably lower $t_{1/2}$ values and higher growth rates were observed for PP/PET (curve A) as compared to PP-*g*-MA/PET (curve B) (containing 10 wt% MA). Although, the $t_{1/2}$ values for latter case decrease as compared to pure PP, it is practically constant with the increase in PET fibre concentration up to 11 wt%.

Fig. 14 shows the variation of crystallinity for PP-*g*-MA/PET as a function of PET fibre content determined from XRD curves. Curves A and B show the crystallinity of PP/PET and PP-*g*-MA/PET, respectively. Higher crystallinity values of the order of 75% are observed for PP/PET compared to 62% for PP-*g*-MA/PET.

These findings can be explained as follows: the maleic anhydride is a well-known compatibilizer for PP/PET system. During the melting process, one end of MA grafts to PP and the other end of carboxylic group allow hydrogen bonding with the PET fibre. The presence of both PET fibre and MA reduce the segmental motion of PP due to which the growth of crystallites is restricted giving rise to small crystallite or spherulite size (see Fig. 10). Additionally, MA does not allow the PET fibre to actively initiate nucleation of PP and hence no transcrystalline morphology is observed. These factors together contribute to lower crystalline values as observed above.

The DSC thermograms of these samples were investigated

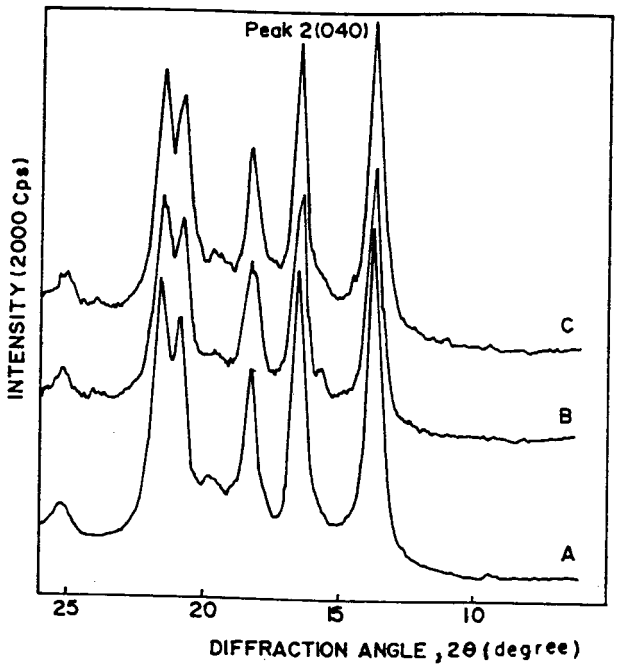

Fig. 11. WAXD scans for PP-*g*-MA/PET (7% PET fibre). Curves A–C correspond to MA concentration of 5, 10 and 15 wt%.

in order to study the difference between the transcrystalline layer of PP/PET and that of PP-*g*-MA/PET, which are shown in Fig. 15a and b. It can be seen from the figures that PP/PET exhibits an exothermic peak at 121°C while that of PP-*g*-MA/PET exhibits an endothermic peak at 118°C, respectively. The increase in crystallisation temperature in the former case as compared to latter can be attributed to PET acting as a strong nucleating agent for PP giving rise to transcrystalline morphology. The presence of transcrystallinity can be clearly observed in the endotherm of

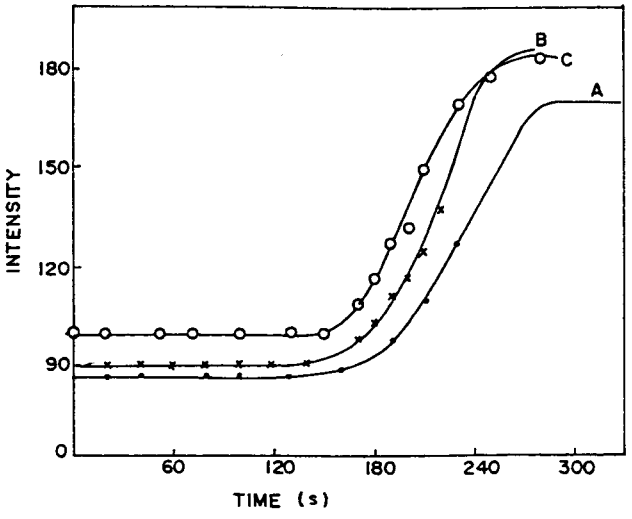

Fig. 12. Crystallisation behaviour (intensity as a function of time) for PP-*g*-MA/PET (10% MA). Curves A, B and C correspond to PET fibre concentration of 4, 7 and 11 wt%.

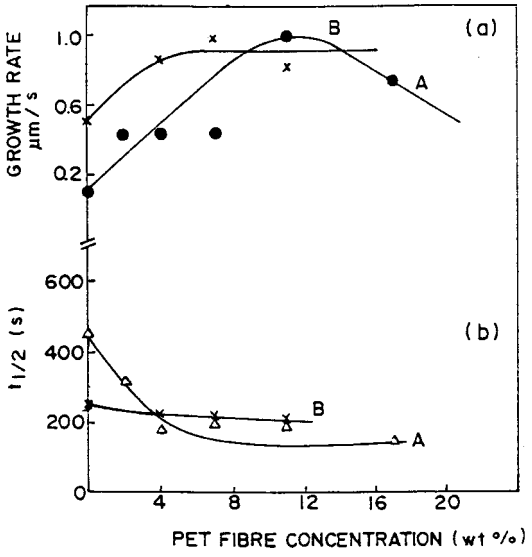

Fig. 13. Crystallisation half time, $t_{1/2}$ (a) and growth rate (b) of PP as a function of PET fibre content. Curve A = PP/PET and curve B = PP/PET containing 10 wt% MA.

PP/PET, which shows a broad peak having a total ΔH value of 145.38 J/g. This broad peak is divided into two peaks; the lower peak has a ΔH of 58.8 J/g which corresponds to transcrystalline zone (fast crystallisation process) giving rise to small spherulites along the fibre surface while the ΔH of 86.5 J/g corresponds to big spherulites away from fibre surface. Thus a total of 145.38 J/g contributes to high crystallinity in PP. On the other hand, a single endothermic peak is observed for PP-*g*-MA/PET having a ΔH of 132.22 J/g. This clearly indicates that the presence of MA prevents the formation of transcrystalline growth of PP spherulites on the surface of PET.

In order to investigate the fibre–matrix interaction, the melt extruded PP/PET composites were examined for SEM after sectioning along the transverse direction. Fig. 16 shows the SEM micrographs for PP/PET (Fig. 16a and b) and PP-*g*-MA/PET (Fig. 16c). The fibre pull out is clearly seen in PP/PET sample (Fig. 16a) suggesting a weak adhesion between the PET fibres and PP matrix. In Fig. 16b, the PET fibres are seen to be surrounded by a thin region near the fibre– matrix interface. This thin layer can be attributed to transcrystalline phase of PP occurring at the interface. On the other hand the micrograph of PP-*g*-MA/PET (Fig. 16c) shows strong fibre matrix adhesion with very little fibre pull out. Thus, we can say that maleic anhydride acts as a good compatibilizer or wetting agent [31–33]. It wets PET fibre and grafts PP matrix to it. There is no transcrystalline zone observed in the presence of MA.

3.3. Measurement of mechanical properties

The mechanical properties, viz. Impact and tensile modulus were evaluated for injection molded samples. Fig. 17a–c

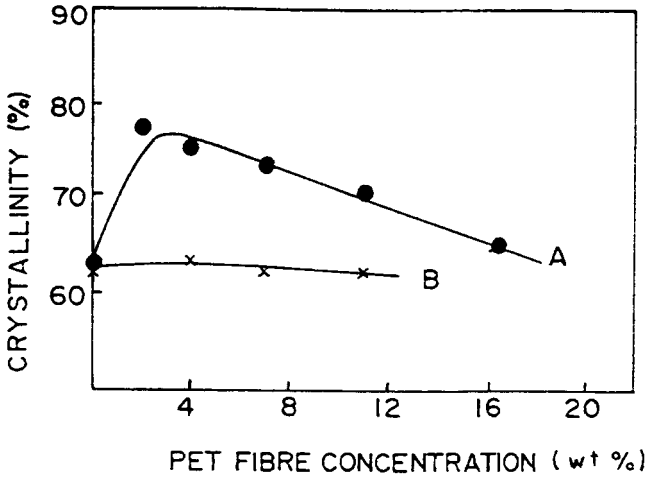

Fig. 14. The variation of crystallinity (%) for PET fibre filled PP composite as a function of fibre content. Curve A = PP/PET and curve B = PP/PET containing 10 wt% MA.

show the typical stress–strain curves for PP, PP containing 10 wt% PET without and with 10 wt% MA. The various properties such as stress at auto break, load at maximum load, strain at break, tensile modulus, etc. are indicated in Table 1. for these composites. (About 8–10 samples were analysed but only their average values are indicated in the table.) From the stress–strain curves, it can be seen that pure PP exhibits a well-defined yield point while PP/PET with and without MA break with no well defined yield point. Also, in case of PP-*g*-MA/PET the strain is considerably high as compared to PP/PET composite.

Fig. 18 shows the variation of tensile modulus with PET fibre concentration. The experimental values have been compared with those expected for a blend PP/PET with and without MA. The expected values were evaluated assuming a non-interactive PP/PET blend having uniform spherical domains of PET dispersed in PP and using a simple rule of mixtures as [34]

$$E_c = \phi_A E_A + \phi_B E_B \quad (3)$$

where E_c is the combined modulus of both PET (globular form) and PP, E_A and E_B are the tensile modulus of PET (globular) as 2758 MPa [35] and PP as 1372 MPa, respectively. The ϕ_A and ϕ_B are the volume fractions of corresponding PET and PP, respectively. In case of PP-*g*-MA/PET, the value of E_B taken for maleated PP is 1288 Mpa rather than that of pure PP. These values have been experimentally determined in our laboratory separately. In Fig. 18 curves A and C correspond to expected modulus values for PP/PET with MA and PP/PET without MA. The curve B corresponds to experimental modulus values for PP/PET with MA and the curve D corresponds to experimental modulus values for PP/PET without MA. There is a considerable increase of tensile modulus in presence of PET fibres

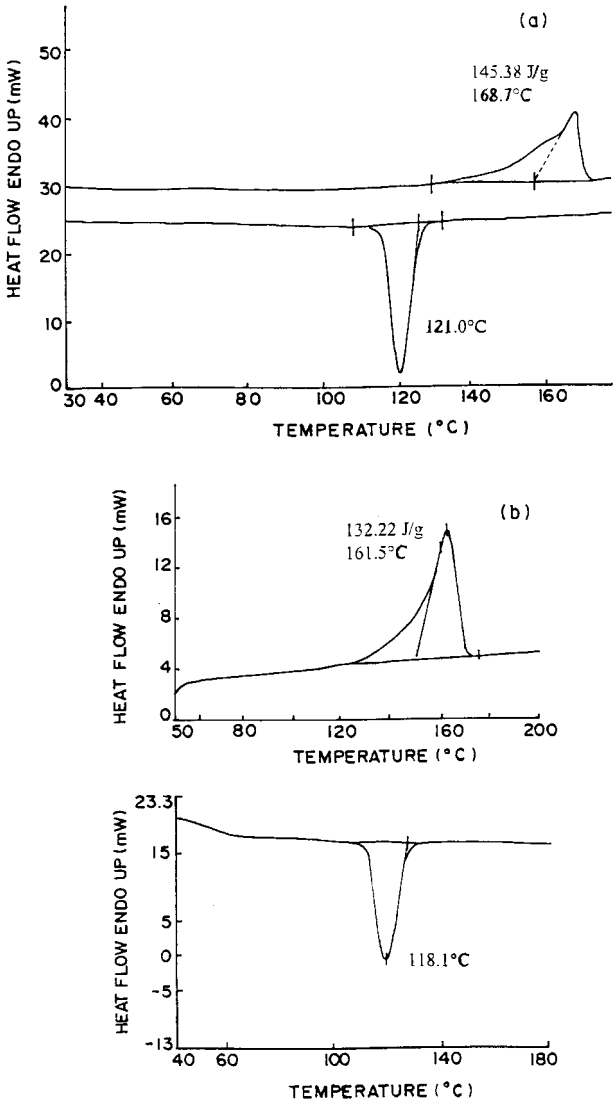

Fig. 15. DSC curves for: (a) PP with 7 wt% PET; (b) PP with 7 wt% PET containing 10 wt% MA both isothermally crystallised at 115°C.

in PP with and without MA as compared to the matrix alone (pure PP or PP/MA).

The increase of tensile modulus in PP/PET fibre composites can be because of: (a) reinforcing effect of PET fibres; (b) higher crystallinity; and (c) transcrystallinity. It is seen that although PET by itself has higher modulus than PP, its blend as a simple dispersed system does not show much improvement as noted in the present case. The fibrous nature with high aspect ratio certainly plays an important role. Further, PP/PET has higher crystallinity (75%) as compared to PP homopolymers (62%). Finally the increase of modulus value can originate from the transcrystalline morphology, which tends to be columnar crystalline structure at the fibre–matrix interface leading to a better interaction between the matrix and the fibres.

Increase of modulus values for PP-*g*-MA/PET as

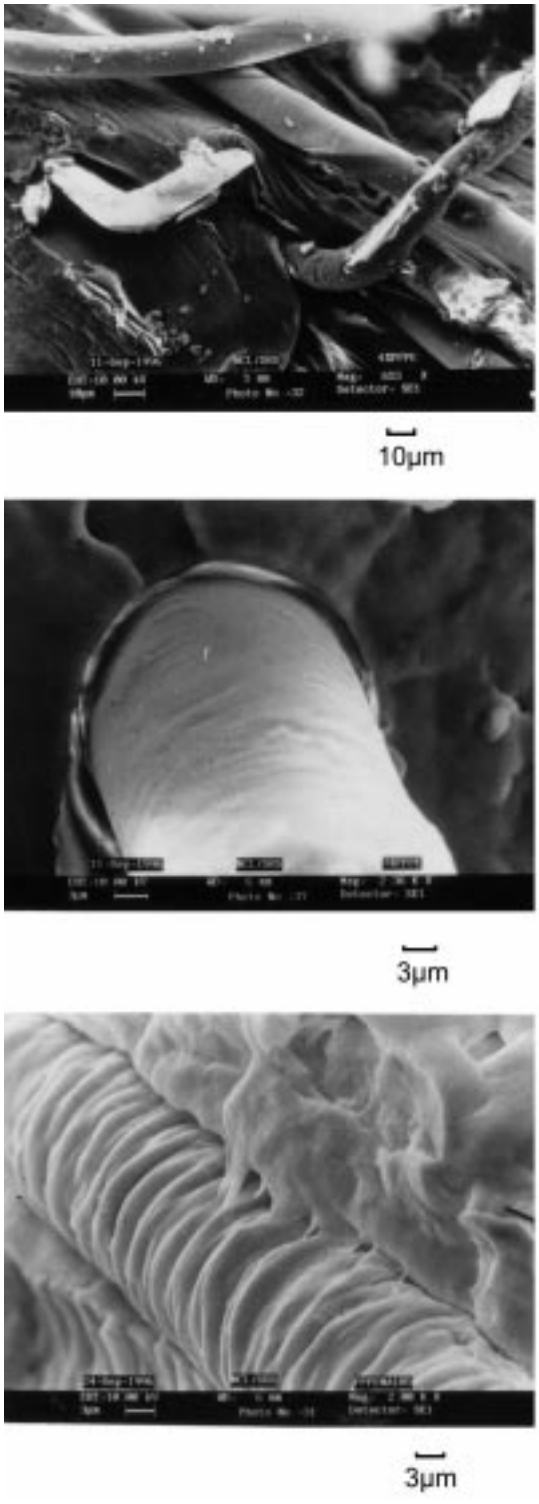

Fig. 16. SEM micrographs of melt extruded samples sectioned along transverse direction. PP with 10% PET (b) PP with 7 wt% PET and (c) PP with 10 wt% PET containing 5% MA.

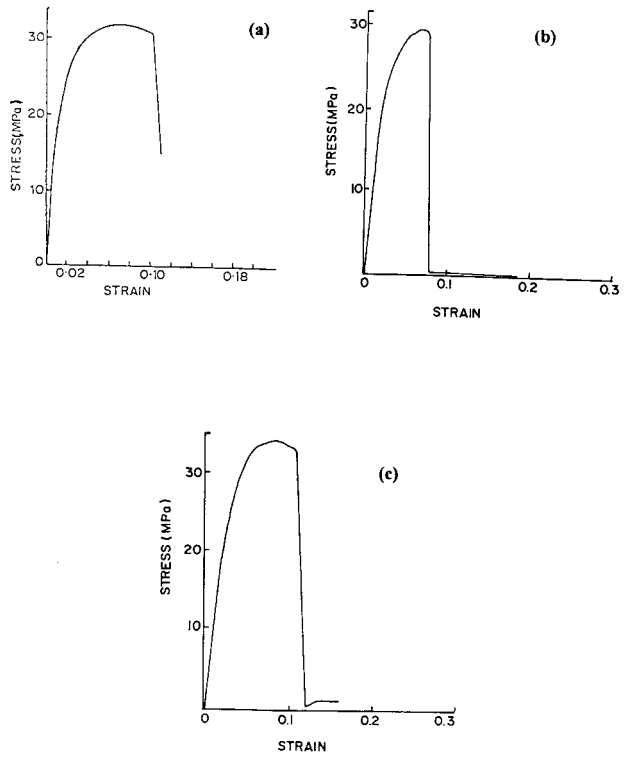

Fig. 17. Graph of stress Vs strain for: (a) pure PP; (b) PP with 10 wt% PET; and (c) PP with 10 wt% PET containing 10 wt% MA.

compared to their expected values can be attributed to: (a) good interfacial adhesion between fibre; and (b) reinforcement effect of PET fibre. It is well known that maleic anhydride grafted on a polymer acts as a good wetting agent and has been used as a compatibilizer for many polymers. As observed earlier in the presence of maleic anhydride the strong interfacial adhesion between the PET fibre and the matrix is achieved. Secondly, as explained earlier the high aspect ratio of PET fibre contributes to an increase of modulus values which are calculated for globular PET.

It is also interesting to note that the modulus value is higher for PP/PET compared to PP-*g*-MA/PET at the same PET fibre concentration. This is due to transcrystalline morphology observed in the former case and its absence in the latter.

From the various reports on the effect of transcrystallinity on the interfacial adhesion in composite materials, it has been found that different views exist with different groups. Some authors [36,37] showed that the fibre–matrix bond strength reduced after the generation of transcrystallinity around the fibres giving rise to poor composite properties while the others [38] have found that it makes little difference to adhesion. However, Schornhorn et al. [39] have shown that if transcrystalline layers are strong it may be advantages in achieving good adhesion. Our results are in good agreement with their observations. Our results indicate that there is an optimum concentration (~7 wt%) of PET fibres at which there is a considerable improvement in the tensile modulus while for higher concentrations the tensile modulus tends to decrease. This may be explained as follows. At low concentrations of PET fibres, the transcrystallinity region is well developed

Table 1
Tensile properties of PP/PET and PP-*g*-MA/PET composites

Composition	Stress at auto break (MPa)	Strain at auto break (%)	Stress at max.load (MPa)	Strain at max. load (%)	Displacement at max. load (mm)	Load at max. load (kN)	Strain at max. load (mm/mm)	Load at auto break (KN)	Displacement at auto break (mm)	Modulus (MPa)
PP	9.17	123.70	30.16	9.81	4.89	1.70	0.09	0.35	61.85	1372
PPPE 2 wt% = PP containing 2 wt% PET	22.91	3.02	22.98	3.16	1.17	0.08	0.03	0.08	1.21	1421
PPPE 3 wt% = PP containing 3 wt% PET	21.04	2.43	24.02	2.85	1.09	0.07	0.02	0.06	0.92	1601
PPPE 7 wt% = PP containing 7 wt% PET	0.77	0.33	21.54	1.98	0.72	0.08	0.01	0.00	0.07	1769
PPPE 8 wt% = PP containing 8 wt% PET	26.12	4.15	29.28	4.19	1.59	0.11	0.04	0.10	1.57	1634
PPPE 10 wt% = PP containing 10 wt% PET	24.68	5.58	25.07	4.83	1.88	0.09	0.04	0.09	2.18	1571
PEM 4 wt% = PP with 4 wt% PET containing 10 wt% MA	29.37	29.61	31.18	31.91	36.70	1.22	0.31	1.15	34.06	1542
PEM 9 wt% = PP with 9 wt% PET containing 10 wt% MA	28.08	36.31	29.03	37.16	42.74	1.12	0.37	1.09	41.76	1566
PEM 14 wt% = PP with 14 wt% PET containing 10 wt% MA	25.10	40.06	25.52	40.50	46.57	1.02	0.40	1.01	46.08	1601
PM 10 wt% = PP containing 10 wt% MA	21.78	23.58	27.62	31.74	36.50	1.05	0.31	0.82	27.12	1288

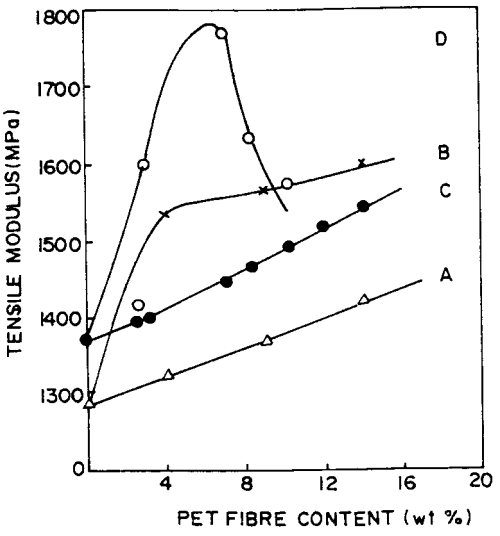

Fig. 18. The tensile modulus for PP/PET composites as a function of PET fibre content according to simple rule of mixture and comparison with the actual data. Curves A and C correspond to expected modulus values for PP/PET with and without MA according to Eq. (3) while curves B and D correspond to experimental modulus for the same system.

Table 2
Izod impact strength of PP/PET and PP-*g*-MA/PET composites

Composition	Izod impact strength notched (J/m)
Pure PP	85
PP with 4 wt% PET	108
PP with 9 wt% PET	117
PP with 14 wt% PET	123
PP with 4 wt% PET containing 10 wt% MA	116
PP with 6 wt% PET containing 10 wt% MA	120
PP with 9 wt% PET containing 10 wt% MA	96
PP with 14 wt% PET containing 10 wt% MA	90

and extends to great extent between the PET fibres. On the other hand, when the PET fibre concentration is high, the fibres are very close to each other and do not allow the full development/or extension of transcrystalline region. Thus, there are weak points in the regions between those PET fibres, which are close to each other. This causes reduction in the tensile modulus at higher PET contents than the optimum concentration.

The impact properties of these composites (notched impact values) are shown in Table 2. It can be observed from the table that both PP/PET and PP-*g*-MA/PET show increase of impact strength as compared to pure PP (85 J/m). The increase is almost 1.4 times than that of pure PP. In case of PP/PET, the impact strength increases with the increase of fibre concentration up to 14 wt% while that for PP-*g*-MA/PET, it increases up to PET content of 6 wt% and tends to decrease slightly with the further increase in fibre concentration. These results can be explained on the basis of spherulite size, bonding between the fibre and matrix and the defects or stress points in the thermoplastic material containing excess fibres (as discussed above). For all these samples, the size of spherulites is considerably small as compared to that in pure PP. Owing to smaller the size of spherulite, the flexibility is higher and hence the impact strength is also high

4. Conclusions

In these studies, we have established that PET fibres influence the crystallisation of PP through crystal–crystal interaction. PET fibres induce row nucleation for PP spherulites giving rise to transcrystalline growth. On the other hand, the presence of MA prevents the formation of transcrystalline growth of PP on the surface of PET fibres but at the same time gives strong fibre–matrix bonding which affects the mechanical properties of the composites as well. Thus, the influence of fibre on PP matrix and vice versa is seen giving an improvement in the mechanical properties of the PP composites.

References

[1] Clegg DW, Collyer AA, editors. Mechanical properties of reinforced thermoplastics. London: Elsevier, 1986 (p. 2).
[2] Krautz FG. J Soc Plast Engng 1971;27:74.
[3] Burton RH, Folkes MJ. Plast Rubber Process Appl 1983;3:29.
[4] Titow WB, Lanham BJ. Reinforced thermoplastics. London: Applied Science Publishers, 1975 (chap. 2; p. 18).
[5] Morristown NJ. Reinforced Capron, Nylon for injection moulding. CL-300-884, Allied Corporation.
[6] Thomason JL, Van Rooyen AA. J Mater Sci 1992;27:5.
[7] Campbell D, Qayyum MM. J Polym Sci, Poly Phys Ed 1980;18:83.
[8] Disalvo AL. J Polym Sci, Polym Lett Ed 1974;12:509.
[9] Chatterjee AM, Price FP, Newman S. J Polym Sci, Polym Phys Ed 1975;13:2369.
[10] Idem. J Polym Sci, Polym Phys Ed 1975;13:2385.
[11] Idem. J Polym Sci, Polym Phys Ed 1975;13:2391.
[12] Saujanya C, Radhakrishnan S. Macromol Mater Engng 2000 (in press).
[13] Hsiao BS, Chen EJH. In: Ishida H, editor. Controlled interphases in composite materials: Amsterdam: Elsevier, 1990 p. 613.
[14] Bessel T, Shortall JB. J Mater Sci 1975;10:2035.
[15] Bussi P, Ishida H. In: Ishida H, editor. Controlled interphases in composite materials: Amsterdam: Elsevier, 1990 p. 391.
[16] He T, Porter RS. J Appl Polym Sci 1988;35:1945.
[17] Peacock JA, Fiffe B, Nield SE, Barow CY. In: Ishida H, Koenig JL, editors. Composite interfaces. Amsterdam: Elsevier, 1986 (p. 143).
[18] Hartness JT. SAMPEJ 1984;20:66.
[19] Lee Y, Porter RS. Polym Engng Sci 1986;26:633.
[20] Misra A, Deopura BL, Xavier SF, Hartley FD, Peters RH. Angew Makromol Chem 1983;113:113.
[21] Radhakrishnan S, Schultz JM. J Cryst Growth 1975;116:459.
[22] Radhakrishnan S, Saini DR. J Cryst Growth 1993;129:191.
[23] Radhakrishnan S, Mandale AB. Synth Met 1994;62:217.
[24] Saujanya C, Radhakrishnan S. J Mater Sci 2000;35:1.
[25] Annual Book of ASTM standards, 1973, Part 27. p. 72.
[26] Annual Book of ASTM standards, 1973, Part 27. p. 192.

[27] Radhakrishnan S, Tapale M, Rairkar E, Shirodkar V, Natu HP. J Appl Polym Sci 1977;64:1247.
[28] Saujanya C, Doni S, Radhakrishnan S. Proceedings of the Macro'98, vol. 2. New Delhi: Allied Publishers, 1998 (85 p).
[29] Madelkern L. Crystallisation in polymers. New York: McGraw Hill, 1964.
[30] Turnbull D, Vonnegut B. Ind Engng Chem 1952;44:1292.
[31] Chen C, Fontan E, Min K, White FL. Polym Engng Sci 1988;28:69.
[32] Ide F, Hasegawa A. J Appl Polym Sci 1974;18:963.
[33] Kim BK, Park SY, Park SJ. Eur Polym J 1991;27:349.
[34] Folkes MJ, Hope PS. Polymer blends and alloys. London: Chapman and Hall, 1993 (chap. 6).
[35] Billmeyer FW. Textbook of polymer science. New York: Wiley, 1984.
[36] Folkes MJ, Hardwick ST, Wong WK. Polymer composites. Proceedings of the 28th Microsymposium on Macromolecules, Prague, July 1985. Berlin: Walter de Gruyter. p. 33.
[37] Huson MJ, Mc Gill WJ. Polym Phys Ed 1985;22:121.
[38] Masouka M, Int J. Int J Adhes Adhesives 1981;1:256.
[39] Kwei TK, Schonhorn H, Frish HL. J Appl Phys 1967;38:2512.